Solar Energy Materials and Solar Cells 173 (2017) 120–127

Contents lists available at ScienceDirect

Solar Energy Materials and Solar Cells

journal homepage: www.elsevier.com/locate/solmat

# Full recovery of red zone in p-type high-performance multicrystalline silicon

Ville Vähänissi*, Hannu S. Laine, Zhengjun Liu, Marko Yli-Koski, Antti Haarahiltunen, Hele Savin

*Aalto University, Department of Electronics and Nanoengineering, Tietotie 3, 02150, Espoo, Finland*

ARTICLE INFO

*Keywords:*
P-type high-performance mc-Si
Lifetime
Dissolution
Gettering
Red zone
Iron

ABSTRACT

Between 10% and 30% of commercial cast silicon ingots is discarded due to contamination caused by the casting process. A significant contaminant in the scrap volume is metal precipitates, which are difficult to getter effectively and degrade minority charge carrier lifetime, hence limiting solar cell efficiency potential. We show here that the unusable red zone can be restored in high-performance multicrystalline silicon wafers. Adding a high temperature dissolution anneal prior to phosphorus diffusion dissolves the metal precipitates within the wafer bulk, and leaves the metal point defects in a mobile state to be readily gettered by phosphorus diffusion gettering during the solar cell process. The efficiency of the dissolution gettering treatment increases with increasing temperature, with a temperature of 1150 °C eliminating the very low lifetime region of the wafers completely. Additionally, we find that the red zone does not re-emerge after a 60 min oxidation anneal at 900 °C, confirming that the achieved benefit is tolerant to any high temperature processing following the phosphorus diffusion gettering process.

## 1. Introduction

The most common wafer material of today's photovoltaic market is multicrystalline silicon (mc-Si), comprising roughly 65% of the market at the end of 2015 [1]. Typically mc-Si ingots are grown inside a quartz crucible by casting or directional solidification methods [2]. Recent advances in these methods have led to the emergence of the very promising high-performance mc-Si (hpmc-Si), a material with lower dislocation cluster density and thus higher quality than conventional mc-Si. [3,4] However, unintentional impurity contamination via diffusion from the crucible during high temperature ingot growth still causes major problems with these crystal growth methods, also in the case of hpmc-Si [5]. As a result, a significant fraction of the ingot volume is discarded, resulting in yields of around 70% in generation 5 ingots [6], which consist of a total of 25 (5 × 5) 15.6 × 15.6 $cm^2$ sized bricks. The discarded material is typically labeled as the red zone.

One of the most detrimental recombination active impurities in silicon, iron, is believed to be the main impurity causing this low lifetime. Considerable concentrations of iron, both in interstitial and precipitated form, have been detected in the red zone [7–10]. Moreover, iron has been shown to be detrimental in edge regions of n-type silicon ingots [11].

The most common method for reducing the impact of iron, and thus also the red zone, in solar cell industry, is phosphorus diffusion gettering (PDG). PDG occurs naturally during emitter formation in p-type silicon solar cells and is well-known to act effectively against interstitial iron ($Fe_i$) [12–14], especially if combined with a following low temperature tail [15–18]. Precipitated impurities, on the other hand, are more problematic. PDG is still rather efficient against relatively small precipitates due to their fast dissolution at typical diffusion temperatures [19]. However, larger precipitates are more difficult to remove. Large precipitates dissolve much slower than smaller ones and therefore are hardly depleted during standard emitter formation [19,20]. In addition to acting as recombination centers, these large precipitates remaining in the wafers cause problems also during the post-PDG high temperature process steps, e.g. contact firing [21] or thermal oxidation [22]. At high temperatures, the remaining precipitates start to dissolve and thus poison their nearby areas by injecting significant amount of $Fe_i$ to their surroundings, killing the minority carrier lifetime [21,23,24,25].

To make gettering effective against large precipitates, so-called dissolution-gettering idea has been proposed [26]. In dissolution-gettering, a high temperature step is employed first to fully dissolve precipitates and subsequently a lower temperature step is implemented to reduce the dissolved iron concentration [$Fe_i$]. The dissolution-gettering idea is partly inspired by the Tabula Rasa process used by the IC-industry to mitigate as-grown oxygen precipitate nuclei [27]. In addition to simulations [21,26,28], the dissolution-gettering idea has also been tried experimentally [28–34], but so far with inconclusive results. Both higher diffusion temperatures [29–33] and separate high temperature dissolution and diffusion steps [28,33,34] have been tested. For example, Ballif et al. [29], Möller et al. [2], and Macdonald

* Corresponding author.
*E-mail address:* ville.vahanissi@aalto.fi (V. Vähänissi).

http://dx.doi.org/10.1016/j.solmat.2017.05.016
Received 17 March 2017; Received in revised form 24 April 2017; Accepted 7 May 2017
Available online 20 May 2017

and Cuevas [30] have reported lower lifetimes in mc-Si after gettering at high temperatures (900–1200 °C). On the other hand, Fenning et al. [33], Morishige et al. [35] and Macdonald et al. [31] observed dissolution of precipitates at microscopic level by synchrotron-based micro-X-ray-fluorescence and also lifetime improvement when increasing the gettering temperatures from 820 °C to 870–880 °C. Michl et al. also reported lifetime improvements after adding a 900 °C dissolution peak prior to a gettering step [28]. The benefit was pronounced especially if also further high temperature steps of the cell process (e.g. contact co-firing) were included in the time-temperature profile.

Our goal here is to solve the considerable problem of red zone by utilizing the dissolution-gettering idea. We systematically study the effect of a pre-PDG dissolution step with a temperature of 900–1150 °C on p-type high performance mc-Si wafers containing a large red zone. To our knowledge, this is the first time high temperature gettering is studied on modern, industrial, high-performance multicrystalline silicon [5], and one of the first reported gettering tests performed on HPMC-Si in general [36]. The impact of the treatments is characterized by lifetime and iron-boron pair measurements. The possible effects of the high temperature anneal on the crystal structure [30] are characterized by etch pit density measurements. For selected wafers, also the thermal stability was studied by an emitter etch back and a subsequent high temperature anneal.

## 2. Experimental

p-type high-performance mc-Si wafers with a thickness of 200 μm, a resistivity of approximately 2 Ωcm, and a size of 7.8×7.8 $cm^2$ were used in this study. The wafers were taken from a corner position brick of an industrial 5-gen ingot, i.e. the wafers contained a large red zone. With a minority carrier lifetime limit of < 20 μs, the width of the red zone was determined to be between 4.5 cm and 5 cm. All the wafers originated from an ingot height distribution of a few centimeters around 30% ingot height.

Processing began by an SC1 clean and a diluted HF-dip. The next process step was a high temperature anneal with varying time and temperature. The process step ended with a rapid cooldown by a direct pullout to room temperature. This process step is later on referred to as the first dissolution treatment. To protect the wafers from possible furnace contamination at high temperatures, the high temperature anneal began with a dry oxidation and nitrogen anneal at 900 °C for 60 min. Fig. 1 depicts the time-temperature profile of the whole experiment including the detailed parameters of the high temperature anneal.

After the first dissolution treatment, the oxide grown on the wafers was etched away in a diluted HF solution. Then the wafers were divided into two groups: i) wafers experiencing PDG and ii) wafers not experiencing PDG. Also as-grown reference wafers, which did not experience the first dissolution treatment, were added to both groups. The PDG treatment comprised a 60-min diffusion step at 870 °C followed by a low temperature tail of 1.5 h at 700 °C. Filmtronics P509 spin-on dopant acted as the phosphorus source. After PDG, the phosphorus glass was removed in a diluted HF solution and the sheet resistance was measured to be approximately 25 Ω/sq.

Subsequently, all the wafers experienced surface etching to remove the heavily phosphorus doped emitter and thus enable meaningful bulk lifetime characterization later on. The surface etching was done in a $CH_3COOH:HF:HNO_3$ solution, and the thickness of the etched layer was approximately 12 μm. Next, the wafers were cleaned again in an SC1 solution and dipped in a diluted HF solution. Finally, the wafer surfaces were passivated by growing a 22-nm-thick $Al_2O_3$ film by atomic layer deposition (ALD) and annealing them for 30 min at 400 °C in a nitrogen atmosphere.

The minority carrier lifetimes in all samples were measured with microwave detected photoconductance decay (μ-PCD). During the first measurement, interstitial iron in the wafers was paired with boron ($Fe_iB_s$). Next, the pairs were dissociated by illumination and the minority carrier lifetime was re-measured. The interstitial iron concentration ($[Fe_i]$) in the wafers was determined from these measurements with the method described in more detail in [37,38]. For selected samples etch pit density (EPD) was determined by a Sopori etching treatment and optical microscopy. The etch pits were registered using an algorithm which has been determined to be accurate to within 10% in comparison with manual counting of the etch pits.

Finally, in order to determine the tolerance to post-PDG high temperature processing, and to reveal the final total $[Fe_i]$ in the wafers, the passivating $Al_2O_3$ layer was etched away in a diluted HF solution and the wafers were cleaned in an SC1 solution and dipped in a diluted HF solution. Next processing step was thermal oxidation, later on referred to as the second dissolution treatment. The wafers were dry oxidized at 900 °C for 40 min in oxygen atmosphere and subsequently annealed at the same temperature for 20 min in nitrogen atmosphere. The purpose of this was to dissolve all the remaining iron precipitates in the wafer and simultaneously provide surface passivation for the following lifetime characterization. Finally, the wafers were characterized by repeating the minority carrier lifetime and $[Fe_i]$ measurements.

## 3. Results

### 3.1. Effect of conventional PDG

Fig. 2a) presents the minority carrier lifetime, $[Fe_i]$ and EPD maps of a reference wafer, i.e. wafer with no dissolution treatment or gettering. The lifetime map is a typical example of a corner wafer. Due to the crucible contamination during the crystal growth, a distinct red zone with extremely low lifetime forms. This divides the wafer into two regions, middle region (1) with mediocre lifetime (~40 μs) and edge region (2), i.e. the red zone, with low lifetime (~5 μs). These two regions differentiate also in the $[Fe_i]$ map and an anti-correlation between the lifetime and $[Fe_i]$ can be seen: lowest lifetime is measured at locations where $[Fe_i]$ is highest. A deviation from this trend is seen at the very bottom and right edge of the wafer. This region is closest to the

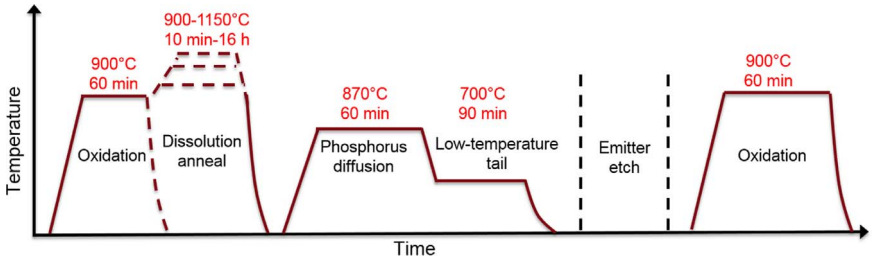


Dissolution anneal parameters

| | | | |
|---|---|---|---|
| oxidation only | 25 min at 950°C | 20 min at 975°C | 15 min at 1000°C |
| 15 min at 1050°C | 10 min at 1100°C | 10 min at 1150°C | 16 h at 1150°C |

**Fig. 1.** The time-temperature profile of the experiment.

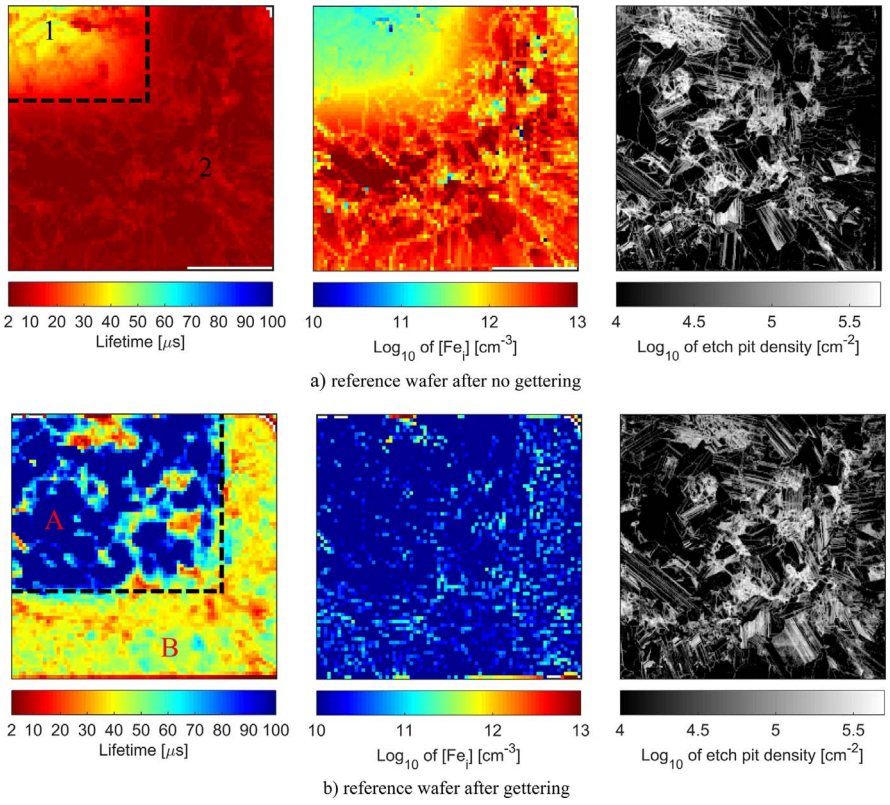


**Fig. 2.** Minority carrier lifetime, [$Fe_i$] and EPD maps of reference wafers after a) no gettering and b) PDG. Sample size is 7.8 × 7.8 $cm^2$.

crucible during the crystal growth, and hence contains the highest total iron concentration. Here, the high iron concentration induces strong iron precipitation, which significantly reduces iron point defects [39], resulting in decreased [$Fe_i$]. The lifetime stays nonetheless low due to recombination at the precipitates [40]. Similar behavior has been observed earlier [7,8,41]. Additionally, in the red zone in areas where EPD is high, [$Fe_i$] seems to be low. This suggests that during crystal cooling dislocations have been decorated, i.e. iron has nucleated to dislocations and the formed precipitates have gettered iron decreasing nearby [$Fe_i$].

Fig. 2b) presents the minority carrier lifetime, [$Fe_i$] and EPD maps of a reference wafer after PDG, i.e. a gettered wafer with no dissolution treatment. The maps exhibit the high efficiency of PDG with a low temperature tail against $Fe_i$. The width of the red zone decreases significantly and simultaneously the lifetime in both areas 1 and 2 improves considerably (~25 μs → ~100 μs and ~5 μs → ~40 μs, respectively). During the 1 h at 870 °C, both $Fe_i$ segregation, as well as dissolution of as-grown iron precipitates occurs. However, 870 °C fails to deplete precipitates [19,42], and therefore, the red zone still remains in the wafer after gettering and is most probably caused by the metal precipitates that PDG failed to remove.

Some areas on the wafer, mostly outside the red zone, seem to exhibit a poor lifetime even after PDG. Comparison of the lifetime and EPD maps reveals, that these areas mostly overlap with areas of high EPD. Dislocations can trap impurities within the dislocation core or in the stress-field they generate [43], hindering the gettering response of dislocated regions [36]. The low lifetime in these areas is thus likely due to recombination-active metal impurities trapped at these dislocations, even after PDG.

Our dissolution-gettering treatment aims to increase the efficiency of a standard PDG especially in the area where the standard PDG fails. For further analysis, we separate this area from the better performing middle region, as noted by areas A and B, respectively in Fig. 2b).

### 3.2. Effect of combined dissolution and gettering

Fig. 3 presents minority carrier lifetime, [$Fe_i$] and EPD maps of selected gettered wafers that have, before gettering, experienced the first dissolution treatment with high temperature anneal parameters of a) 25 min at 950 °C, b) 15 min at 1050 °C, and c) 16 h at 1150 °C. At the low end of the dissolution temperature scale used here, the wafer is still clearly divided into two regions, similarly as after mere gettering (see Fig. 2b)). Whereas the standard gettering treatment reduces the red zone from approximately 51 mm to 26 mm, adding a 25 min pre-PDG dissolution anneal at 950 °C results in a slightly narrower red zone of 23 mm (see Fig. 3). When the dissolution temperature increases further, the benefits of the dissolution anneal grow distinctly. With dissolution temperatures above 1000 °C, the red zone width is decreased down to 2–3 mm, practically eliminating it altogether.

Changes in lifetime occur also in the middle region (area A). As stated earlier, some areas on the wafer seem to have a poor lifetime even after PDG. By comparing the lifetime map to the EPD map, the result is similar than before, these poorly-performing areas mostly overlap with areas of high EPD. It seems thus that the dissolution gettering process is not able to recover the most heavily decorated structural defects.

Dissolution treatment seems to have an impact on the EPD: the higher the peak temperature, the brighter the EPD map appears to be. Although the ingot height also affects the dislocation density, the average EPD density exhibits a stronger increasing trend as a function of increasing dissolution temperature than as a function of increasing ingot height, as discussed later in Section 4.4.

Fig. 4 presents both the arithmetic and the square-root-weighted harmonic mean of minority carrier lifetime ($\frac{1}{\sqrt{\tau_{eff,avg}}} = \frac{1}{n}\sum\frac{1}{\sqrt{\tau_{eff,i}}}$), a strong predictor of final cell performance [44–46] in the red zone (area B) and middle region (area A) after various dissolution treatments followed by gettering. The high temperature anneal has a positive effect on the red zone lifetime, evident in the general trend of increased

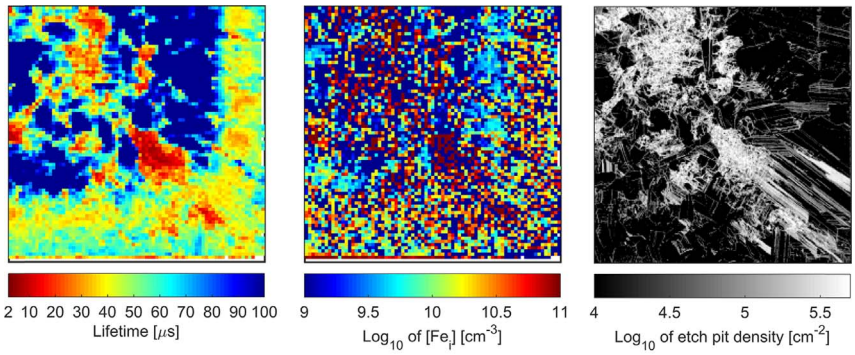


a) 25 min at 950°C

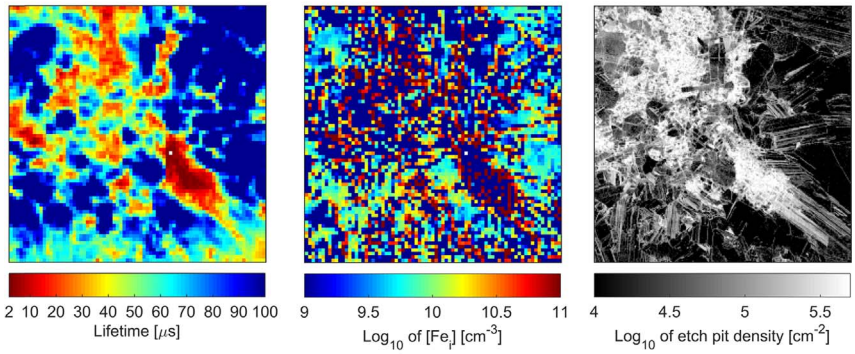


b) 15 min at 1050°C

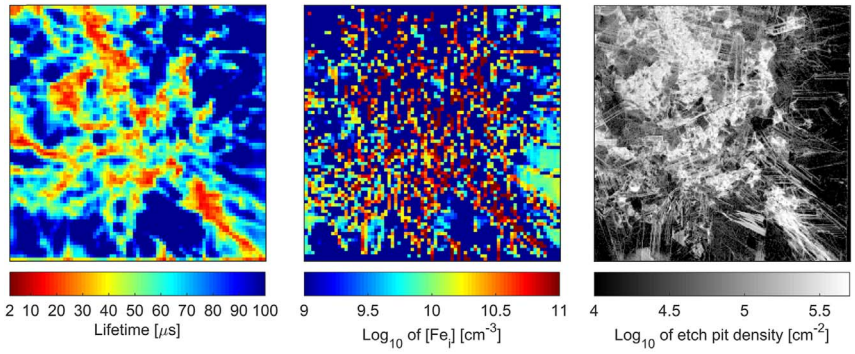


c) 16 h at 1150°C

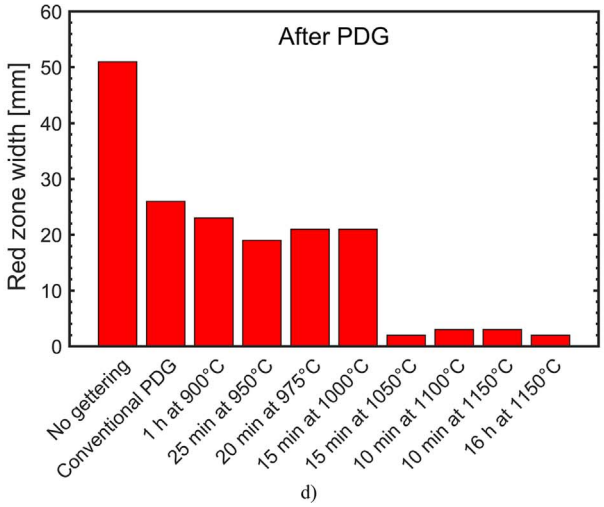


d)

**Fig. 3.** Minority carrier lifetime, [$Fe_i$] and EPD maps of selected gettered wafers that have, before gettering, experienced the first dissolution treatment with high temperature anneal parameters of a) 25 min at 950 °C, b) 15 min at 1050 °C and c) 16 h at 1150 °C. Sample size is $7.8 \times 7.8$ $cm^2$. Also, d) the width of the red zone after various dissolution treatments followed by gettering is shown. The lifetime limit for the red zone is < 50 μs. For reference, the as-grown red-zone width, as defined in Fig. 2, is shown. (For interpretation of the references to color in this figure legend, the reader is referred to the web version of this article).

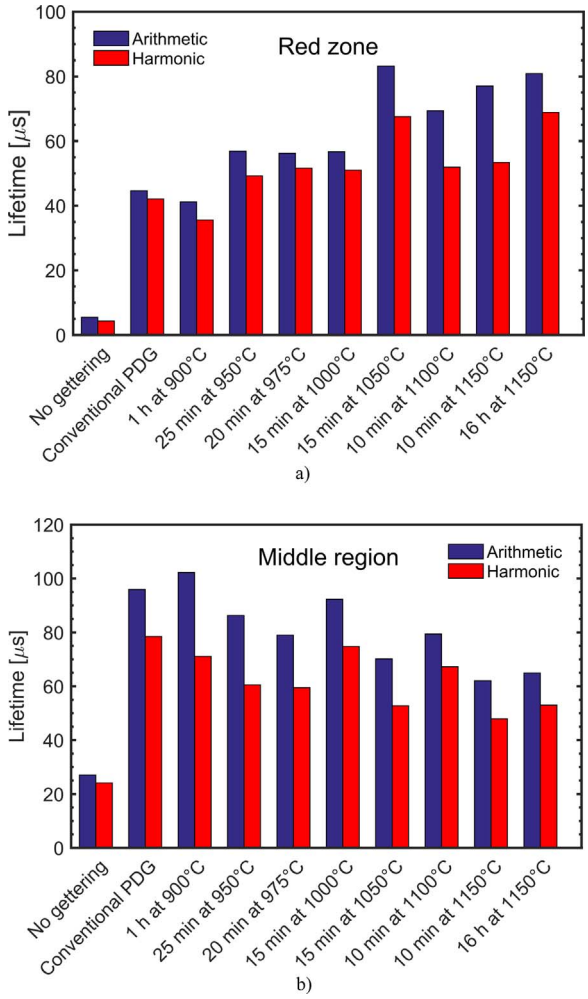


**Fig. 4.** The arithmetic and square-root-weighted harmonic mean of minority carrier lifetime a) in the red zone (area B) and b) middle region (area A) after various dissolution treatments followed by gettering. For definition of red zone and middle region, please refer to Fig. 2. (For interpretation of the references to color in this figure legend, the reader is referred to the web version of this article).

lifetime with increasing dissolution temperature (see Fig. 4a)). At the low end of the temperature scale used here (< 1050 °C), the dissolution treatment brings modest improvements in lifetime, and the arithmetic and harmonic average lifetimes are within 15% of each other. This improvement coincides with the modest decrease in the red zone width observed previously (see Fig. 3d)). At higher dissolution temperatures, the arithmetic average lifetime increases significantly, reaching values almost a factor of two higher compared to conventional PDG (85 μs vs. 45 μs). This result again coincides with the significant decrease in the red zone width (Fig. 4d)). However, the positive effect fails to carry over to the harmonic average lifetime in the same extent, because the lifetime remains poor in dislocated areas, and these poor areas begin to dominate the harmonic average more strongly.

On the other hand, adding the dissolution treatment seems to offer no lifetime benefit in the middle region (Fig. 4b)). On the contrary, both the arithmetic and harmonic lifetime exhibit a slightly decreasing trend as a function of increasing dissolution temperature. The difference between the two averages is also notable, due to a significant proliferation of small, low lifetime areas which coincide with high EPD. However, the lifetime increase compared to the as-grown sample is significant, more than a factor of two, in all processed samples.

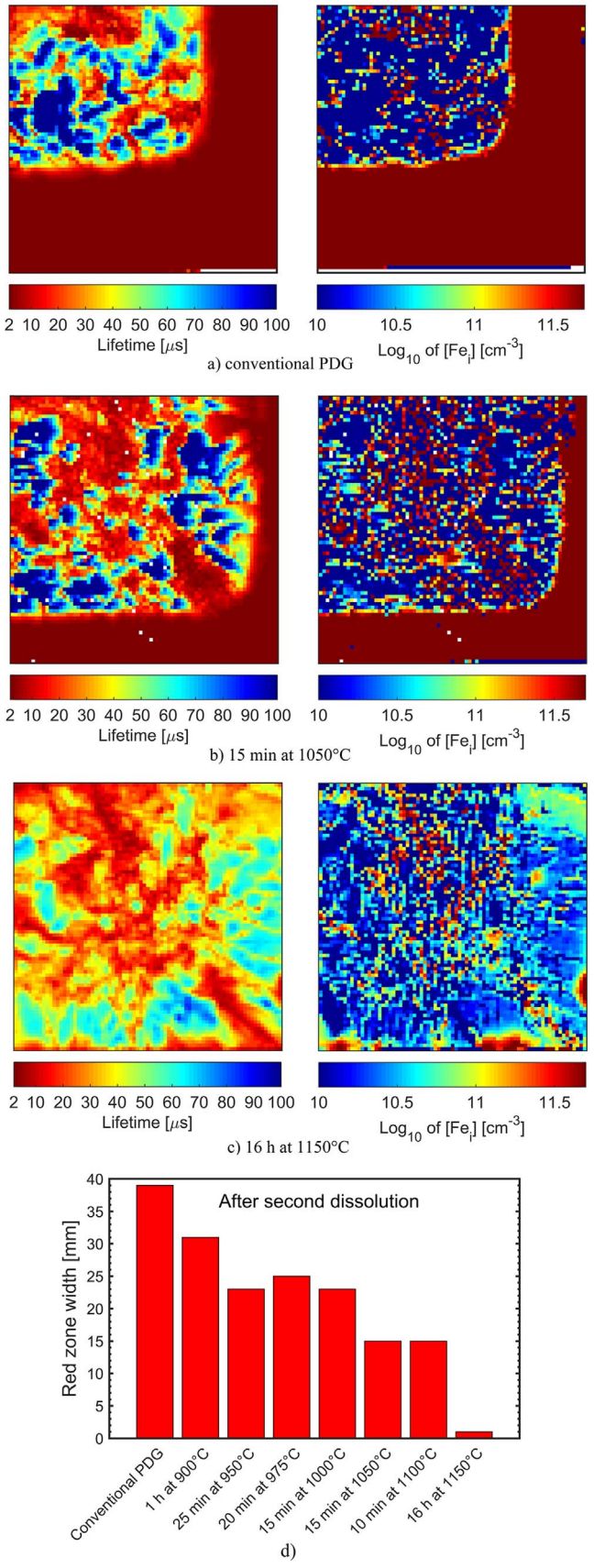


(caption on next page)

**Fig. 5.** Minority carrier lifetime and [$Fe_i$] maps of selected wafers after the second dissolution treatment. Prior to the second dissolution treatment, the wafers experienced either a) conventional gettering or b) and c) combination of dissolution and gettering. The high temperature anneal parameters during the first dissolution treatment for the wafers were b) 15 min at 1050 °C and c) 16 h at 1150 °C. Sample size is 7.8×7.8 $cm^2$. The width of the red zone after the second dissolution treatment is presented in d). The lifetime limit for the red zone is < 50 μs. (For interpretation of the references to color in this figure legend, the reader is referred to the web version of this article).

### 3.3. Tolerance to further high-temperature processing

In order to determine the tolerance of dissolution-gettered wafers to further high temperature processing, e.g. firing, and to reveal the final total [$Fe_i$] in the wafers, selected samples experienced a second dissolution treatment as detailed in the experimental section. Fig. 5 presents the minority carrier lifetime and [$Fe_i$] maps of the selected wafers and the width of the red zone after the second dissolution treatment. Without any pre-PDG dissolution treatment, the lifetime in the remaining red zone area is completely killed by the second dissolution treatment (Fig. 5a)). This is most likely due to considerable amount of precipitated iron remaining in the wafer after mere PDG [19,35], which then upon dissolution deteriorates the lifetime significantly. The dissolution is seen also in the [$Fe_i$] map. However, when adding the pre-PDG high temperature dissolution treatment, the wafers improve. In other words, after dissolution and gettering, the area where the lifetime is totally killed due to the second dissolution treatment is significantly decreased. As seen in Fig. 3, also here, the higher peak temperature in the first dissolution treatment leads to smaller degraded area. In fact, at 1150 °C, the red zone does not practically re-emerge at all. Therefore, it seems that the removal of red zone by the combination of dissolution and gettering presented earlier, is tolerant against any post-PDG high temperature steps, such as thermal oxidation [22] or contact co-firing [21].

The trend in the residual red zone width after the second dissolution (Fig. 5d)) is broadly similar to that before the second dissolution (Fig. 3d)). An important exception is two samples with dissolution treatments of 15 min at 1050 °C and 10 min at 1100 °C. In these samples, the red zone width increases significantly as a result of the second dissolution, from 3 mm to 16 and 12 mm, respectively. This suggests that these samples included a significant amount of very large iron precipitates, which even the 1150 °C anneal fails to fully deplete in 10 min. These precipitates then dissolve upon the second dissolution, deteriorating the lifetime. Recently, we observed a similar trend of decreasing residual red zone width with increasing dissolution treatment temperature for quasi-mono silicon substrates containing a red zone [34].

## 4. Discussion

### 4.1. The lifetime impact and gettering of iron precipitates

The increase in red zone lifetime seems to correlate with the decrease in the total iron concentration, i.e. the more the process is able to reduce the total iron concentration (see Fig. 5d)), the better the red zone lifetime will be (see Fig. 4a)). Low dissolution temperatures are able to reduce the density of iron precipitates but the reduction in the total amount of iron is not that considerable. On the other hand, at high dissolution temperatures, also the reduction in the total amount of iron is significant and therefore the red zone area is decreased and the average lifetime is increased at best to 85 μs compared to 45 μs with gettering without any dissolution anneal.

The decrease in total iron concentration affects the final lifetime in two ways, directly and indirectly. A smaller density of iron precipitates directly increases the lifetime. Even though the effect of iron precipitates to the lifetime is normally small, it stands out after efficient removal of $Fe_i$. The indirect effect is also related to the reduction of the precipitate density. When the density reduces, also the dissolution of iron during PDG is reduced, which results in a lower steady state iron concentration during gettering, thus increasing the lifetime indirectly. This indirect effect may not be that significant in the lifetime measured right after PDG. However, if further high temperature steps, e.g. firing or thermal oxidation, are done, the smaller amount of precipitated iron in the precipitates and lower density of iron precipitates will be seen as a significantly higher lifetime due to smaller amount of dissolving iron during subsequent high temperature processing.

### 4.2. Our results in the context of literature

Our [$Fe_i$] and lifetime results after gettering are in agreement with the work reported by Fenning et al. [33] First, they confirmed that higher-temperature diffusion successfully extracted a greater fraction of precipitated metal content. Second, they also reported a strong lifetime improvement in iron-contaminated p-type mc-Si wafers with higher than standard gettering temperatures and noticed that the increase took place especially in areas of low dislocation density. They studied both gettering at higher temperatures and also a dissolution step preceding gettering. The maximum temperature used in their study was 920 °C. Their material was intentionally iron contaminated to the level of approximately $10^{15}$ atoms/$cm^3$. Compared to their study, we came to similar conclusions for a much wider temperature (between 900 °C and 1150 °C) and contamination scales.

Our lifetime results in the middle region of the wafers, where the lifetime is not initially limited by crucible contamination (Fig. 4b), are similar to those obtained by Scott et al. [47]. They studied PDG at a varying temperature for (non-seed assisted) multicrystalline silicon wafers taken from the top part of the ingot (92% and 95% ingot height), where the crucible contamination is significant. They found, that above a certain temperature (~900 °C), the lifetime no longer increases as the gettering temperature increases. They hypothesized that a defect other than iron, with most likely lower solid solubility and lower diffusivity, is causing the lifetime decrease.

Michl et al. [28] have also studied the influence of different diffusion temperature profiles on [$Fe_i$] and presented results showing the importance of including possible further high temperature steps in a solar cell process, such as firing, into the study. Their results showed that the positive effect of a dissolution peak prior to phosphorus diffusion was strongly emphasized in the post-firing lifetime. The firing step effectively dissolves the possible precipitates remaining in the wafer and as a result, the lifetime distribution after firing can be notably different than that after PDG. Our results support this, as we saw that due to the second dissolution step the red zone strongly reappeared after dissolution-gettering with dissolution temperatures on the low end of our scale (see Fig. 5d)). Similarly, a significant increase in the [$Fe_i$] was seen (see Fig. 5a)-c)). Therefore, we conclude that, at least in heavily contaminated material/corner wafers lifetime and/or [$Fe_i$] after PDG are not necessarily reliable indicators of cell performance whereas the total iron concentration, or more specifically, density and size of iron precipitates, seems to be.

### 4.3. Red zone removal on an industrial solar cell process line

Typical industrial solar cells use an emitter with higher sheet resistance of around 100 Ω/sq. [1] to reduce Auger recombination, whereas we used a sheet resistance around 25 Ω/sq. Since a higher sheet resistance translates to a lower gettering efficiency, the optimal red zone mitigation strategy may differ with a different sheet resistance. If the dissolved iron concentration is too high as a result of the dissolution treatment, it may be that the phosphorus diffusion gettering during the emitter formation is not able to getter all the dissolved iron.

With a higher sheet resistance, also the importance of accounting for all post-PDG high temperature steps increases. A lightly-doped emitter formed at a low temperature may still be efficient in gettering residual

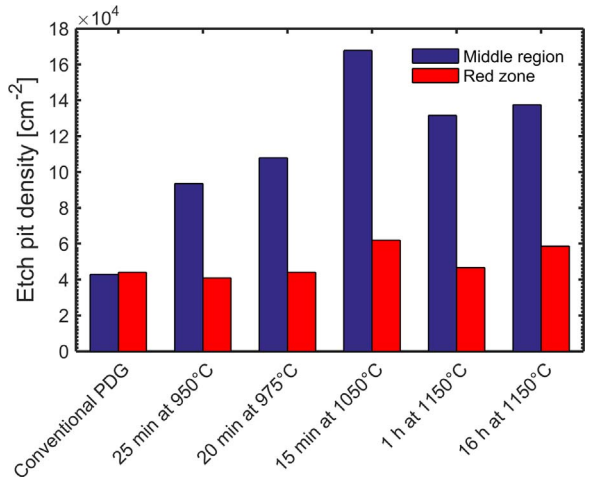


**Fig. 6.** The average etch pit densities measured from the middle region and the red zone of the processed wafers. For definition of middle region and red zone, please refer to Fig. 2. (For interpretation of the references to color in this figure legend, the reader is referred to the web version of this article).

dissolved iron, but may leave a significant fraction of precipitates within the wafer bulk. Upon post-PDG high temperature processing, these precipitates will then dissolve, deteriorating the lifetime of the finished solar cell. However, this effect can likely be mitigated by engineering the contact firing time-temperature profile [25] or via low temperature annealing after PDG [48].

A heavy emitter can also be incorporated into an industrial solar cell process, if part of the highly-doped region is etched back after PDG [49]. As it is likely economical to sort out the red zone wafers altogether for the high-temperature dissolution, it may also be practical to etch away the highly-doped emitter altogether and then place the once-gettered wafers in the same PDG batch with typical non-red zone wafers and re-do a typical industrial emitter on them. With a heavy emitter, residual $Fe_i$ is unlikely to be a problem, and higher dissolution temperatures are likely favoured, at least from the perspective of mitigating iron.

Lastly, we note that the photovoltaic community has recently begun investigating the Tabula Rasa process [27] to mitigate oxygen precipitate nuclei in oxygen-rich Czochralski-silicon [50–52]. Since the temperature range typically studied for Tabula Rasa is similar to what is used here, the Tabula Rasa process can likely be optimized to simultaneously mitigate both oxygen precipitate nuclei and metal precipitates.

### 4.4. Dislocation behavior during processing

Fig. 6 depicts the etch pit density for selected dissolution treatments, and for both the middle region and the red zone region, as defined in Fig. 2. Earlier studies have observed both decrease [53] and increase [30] of dislocation density in multicrystalline silicon during high temperature processing. We observe different trends for the dislocation density behavior in the red zone region and middle region. In the middle region, a higher dissolution temperature correlates with a higher dislocation density, whereas in the red zone, no trend is evident. Also, the dislocation densities are higher in the middle region than in the red zone in all the samples. The dislocation density is known to increase as a function of ingot height. In our case, however, the dislocation density trend is stronger (in the middle region), when plotted as a function of increasing dissolution temperature, than when plotted as a function of increasing ingot height. Moreover, the range of measured dislocation densities is high, from $4\times10^4\ cm^{-2}$ to almost $2\times10^5\ cm^{-2}$.

It could be, that the thermal stress induced by pulling out the wafers from the high temperature furnace, could induce dislocation multiplication. Since especially areas with poor lifetime (Fig. 3a)-c)) coincide with a high dislocation density, controlling the thermal load of the wafers could yield lower dislocation densities, and thus, higher lifetimes. One pathway would be to perform the dissolution and gettering step in the same furnace, which would circumvent the need for a rapid room temperature cool down in between the dissolution and gettering steps.

## 5. Conclusions

Yield loss of multicrystalline silicon ingots caused by crucible contamination is a significant problem in today's photovoltaic industry. We demonstrated here a process to heal the red zone, and turn the minority charge carrier lifetime within the red zone comparable, or higher, to that in uncontaminated regions. More specifically, the arithmetic average lifetime increases from 6 μs to 85 μs in the red zone. Additionally, we find that the red zone does not re-emerge after a 60 min oxidation anneal at 900 °C, confirming that the achieved benefit is tolerant to any high temperature processing following the phosphorus diffusion gettering process.

## Acknowledgements

The authors acknowledge the financial support from the Finnish Funding Agency for Innovation under projects “PASSI” (project No. 2196/31/2011) and “BLACK” (project No. 2956/31/2014), Academy of Finland, Okmetic Oyj and Semilab Inc. The corresponding author thanks Walter Ahlström Foundation for financial support. H. S. Laine acknowledges the financial support of The Finnish Cultural Foundation, the Fulbright Technology Industries of Finland grant, and the Walter Ahlström Foundation. The authors acknowledge the provision of facilities and technical support by Aalto University at Micronova Nanofabrication Centre.

## References

[1] International Technology Roadmap for Photovoltaic (ITRPV), Results, Seventh Edition, ⟨http://www.itrpv.net/Reports/Downloads/⟩, 2016. (Accessed 6 Decemeber 2016), 2015.
[2] H. Möller, C. Funke, M. Rinio, S. Scholz, Multicrystalline silicon for solar cells, Thin Solid Films 487 (2005) 179–187.
[3] Y. Yang, A. Yu, B. Hsu, W. Hsu, A. Yang, C. Lan, Development of high-performance multicrystalline silicon for photovoltaic industry, Prog. Photovolt.: Res. Appl. 23 (2013) 340–351.
[4] X. Tang, L. Francis, L. Gong, F. Wang, J.-P. Raskin, D. Flandre, S. Zhang, D. You, L. Wu, B. Dai, Characterization of high-efficiency multi-crystalline silicon in industrial production, Sol. Energy Mater. Sol. Cells 117 (2013) 225–230.
[5] D. Zhu, L. Ming, M. Huang, Z. Zhang, X. Huang, Seed-assisted growth of high-quality multi-crystalline silicon in directional solidification, J. Cryst. Growth 386 (2014) 52–56.
[6] C. Lan, C. Hsu, K. Nakajima, Multicrystalline silicon crystal growth for photovoltaic applications, Bulk Cryst. Growth: Basic Tech., and Growth Mechanisms and Dyn., Editors: P. Rudolph, pp. 373–412, 2015.
[7] A. Holt, E. Enebakk, A.-.K. Soiland, Effect of impurities in the minority carrier lifetime of silicon made by the metallurgical route, Proceedings of the 22nd Eur. Photovolt. Sol. Energy Conference, Milan, Italy, pp. 1155–1159, 2007.
[8] T.U. Naerland, L. Arnberg, A. Holt, Origin of the low carrier lifetime edge zone in multicrystalline PV silicon, Prog. Photovolt.: Res. Appl. 17 (2009) 289–296.
[9] M.C. Schubert, J. Schön, F. Schindler, W. Kwapil, A. Abdollahinia, B. Michl, S. Riepe, C. Schmid, M. Schumann, S. Meyer, W. Warta, Impact of impurities from crucible and coating on mc-silicon quality—The example of iron and cobalt, J. Photovolt. 3 (2013) 1250–1258.
[10] F. Schindler, B. Michl, J. Schön, W. Kwapil, W. Warta, M.C. Schubert, Solar cell efficiency losses due to impurities from the crucible in multicrystalline silicon, J. Photovolt. 4 (2014) 122–129.
[11] J. Schön, F. Schindler, W. Kwapil, M. Knörlein, P. Krenckel, S. Riepe, W. Warta, M.C. Schubert, Identification of the most relevant metal impurities in mc n-type silicon for solar cells, Sol. Energy Mater. Sol. Cells 142 (2015) 107–115.
[12] A. Bentzen, A. Holt, R. Kopecek, G. Stokkan, J.S. Christensen, B.G. Svensson, Gettering of transition metal impurities during phosphorus emitter diffusion in multicrystalline silicon solar cell processing, J. Appl. Phys. 99 (2006) 093509.
[13] J. Tan, A. Cuevas, D. Macdonald, T. Trupke, R. Bardos, K. Roth, On the electronic improvement of multi-crystalline silicon via gettering and hydrogenation, Prog. Photovolt.: Res. Appl. 16 (2008) 129–134.
[14] D. Macdonald, A. Cuevas, A. Kinomura, Y. Nakano, Phosphorus gettering in

multicrystalline silicon studied by neutron activation analysis, Conference Rec. of the 29th IEEE Photovolt. Specialists, New Orleans, USA, pp. 285–288, 2002.
[15] J. Härkönen, V.-P. Lempinen, T. Juvonen, J. Kylmäluoma, Recovery of minority carrier lifetime in low-cost multicrystalline silicon, Sol. Energy Mater. Sol. Cells 73 (2002) 125–130.
[16] A. Bentzen, E.S. Marstein, R. Kopecek, A. Holt, Phosphorus diffusion and gettering in multi-crystalline silicon solar cell processing, Proceedings of the 19th Eur. Photovolt. Sol. Energy Conference, Paris, France, pp. 935–938, 2004.
[17] P. Manshanden, L.J. Geerligs, Improved phosphorous gettering of multicrystalline silicon, Sol. Energy Mater. Sol. Cells 90 (2006) 998–1012.
[18] A. Peral, J.M. Míguez, R. Ordás, C. del Cañizo, Lifetime improvement after phosphorous diffusion gettering on upgraded metallurgical grade silicon, Sol. Energy Mater. Sol. Cells 130 (2014) 686–689.
[19] D.P. Fenning, J. Hofstetter, M.I. Bertoni, G. Coletti, B. Lai, C. del Cañizo, T. Buonassisi, Precipitated iron: a limit on gettering efficacy in multicrystalline silicon, J. Appl. Phys. 113 (2013) 044521.
[20] J. Schön, A. Haarahiltunen, H. Savin, D. Fenning, T. Buonassisi, W. Warta, M. Schubert, Analyses of the evolution of iron-silicide precipitates in multicrystalline silicon during solar cell processing, J. Photovolt. 3 (2013) 131–137.
[21] J.-F. Lelievre, J. Hofstetter, A. Peral, I. Hoces, F. Recart, C. del Canizo, Dissolution and gettering of iron during contact co-firing, Energy Proc. 8 (2011) 257–262.
[22] S. Mack, U. Jäger, G. Kästner, E.A. Wotke, U. Belledin, A. Wolf, R. Preu, D. Biro, Towards 19% efficient industrial PERC devices using simultaneous front emitter and rear surface passivation by thermal oxidation, Conference Rec. of the 35th IEEE Photovolt. Specialists, Honolulu, USA, pp. 000034–000038, 2010.
[23] S. Hugo, Release of metal impurities from structural defects in polycrystalline silicon, Appl. Phys. Lett. 71 (1997) 1984–1986.
[24] T. Buonassisi, A. Istratov, S. Peters, C. Ballif, J. Isenberg, S. Riepe, W. Warta, R. Schindler, G. Willeke, Z. Lai, B. Lai, E. Weber, Impact of metal silicide precipitate dissolution during rapid thermal processing of multicrystalline silicon solar cells, Appl. Phys. Lett. 87 (2005) 121918.
[25] A. Peral, J.-F. Lelievre, F. Recart, C. del Canizo, Defect engineering during the contact co-firing step in an industrial belt furnace, Phys. Status Solidi C 9 (2012) 2107–2110.
[26] P.S. Plekhanov, R. Gafiteanu, U.M. Gosele, T.Y. Tan, Modeling of gettering of precipitated impurities from Si for carrier lifetime improvement in solar cell applications, J. Appl. Phys. 86 (1999) 2453–2458.
[27] R. Falster, M. Cornara, D. Gambaro, M. Olmo, M. Pagani, Effect of high temperature pre-anneal on oxygen precipitates nucleation kinetics in Si, Solid State Phenom. 57–58 (1997) 123–128.
[28] B. Michl, J. Schön, W. Warta, M. Schubert, The impact of different diffusion temperature profiles on iron concentrations and carrier lifetimes in multicrystalline silicon wafers, J. Photovolt. 3 (2013) 635–640.
[29] C. Ballif, S. Peters, D. Borchert, C. Hässler, J. Isenberg, R. Schindler, W. Warta, G. Willeke, Lifetime investigations of degradation effects in processed multicrystalline silicon wafers, Proceedings of the 17th Eur. Photovolt. Sol. Energy Conference, Munich, Germany, pp. 1818–1821, 2001.
[30] D. Macdonald, A. Cuevas, The trade-off between phosphorus gettering and thermal degradation in multicrystalline silicon, Proceedings of the 16th Eur. Photovolt. Sol. Energy Conference, Glasgow, Scotland, pp. 1707–1710, 2000.
[31] D. Macdonald, S. Phang, F. Rougieux, S. Lim, D. Paterson, D. Howard, M. de Jonge, C. Ryan, Iron-rich particles in heavily contaminated multicrystalline silicon wafers and their response to phosphorus gettering, Semicond. Sci. Technol. 27 (2012) 125016.
[32] V. Osinniy, A. Nylandsted Larsen, E. Hvidsten Dahl, E. Enebakk, A.-K. Søiland, R. Tronstad, Y. Safir, Gettering improvements of minority-carrier lifetimes in solar grade silicon, Sol. Energy Mater. Sol. Cells 101 (2012) 123–130.
[33] D. Fenning, A. Zuschlag, M. Bertoni, B. Lai, G. Hahn, T. Buonassisi, Improved iron gettering of contaminated multicrystalline silicon by high-temperature phosphorus diffusion, J. Appl. Phys. 113 (2013) 214504.
[34] Z. Liu, V. Vähänissi, H.S. Laine, M. Lindeberg, M. Yli-Koski, H. Savin, Electronic quality improvement of highly defective quasi-mono silicon material by phosphorus diffusion gettering, Adv. Electron. Mater., 2017 (In press, <http://dx.doi.org/10.1002/aelm.201600435>), article number 1600435, 6 pages.
[35] A.E. Morishige, M.A. Jensen, J. Hofstetter, P.X.T. Yen, C. Wang, B. Lai, D.P. Fenning, T. Buonassisi, Sycnhrotron-based investigation of transition-metal getteribility in n-type multicrystalline silicon, Appl. Phys. Lett. 108 (2016) 202104.
[36] S. Castellanos, K.E. Ekstrom, A. Autruffe, M.A. Jensen, A.E. Morishige, J. Hofstetter, P. Yen, B. Lai, G. Stokkan, C. del Canizo, T. Buonassisi, High-performance and traditional multicrystalline silicon: comparing gettering responses and lifetime-limiting defects, J. Photovolt. 6 (2016) 632–640.
[37] M. Yli-Koski, M. Palokangas, V. Sokolov, J. Storgårds, H. Väinölä, H. Holmberg, J. Sinkkonen, Recombination activity of iron in boron doped silicon, Phys. Scr. T101 (2002) 86–88.
[38] A. Haarahiltunen, H. Väinölä, M. Yli-Koski, E. Saarnilehto, J. Sinkkonen, Detection of iron contamination in internally gettered p-type silicon wafers by lifetime measurements, The Electrochemical Society Proceedings Vol. 05, High purity silicon VIII, Editors: C.L. Claeys, M. Watanabe, R. Falster, P. Stallhofer, pp. 135–145, 2004.
[39] T. Buonassisi, A.A. Istratov, M.A. Marcus, B. Lai, Z. Cai, S.M. Heald, E.R. Weber, Engineering metal-impurity nanodefects for low-cost solar cells, Nat. Mater. 4 (2005) 676–679.
[40] W. Kwapil, J. Schön, W. Warta, M.C. Schubert, Recombination at metal precipitates in p- and n-type silicon, J. Photovolt. 5 (2015) 1285–1292.
[41] J. Schön, Modellierung von Prozessschritten, zur Umlagerung rekombinationsaktiver Defekte in kristallinem Silizium (Ph.D. Thesis), University of Konstanz, Germany, 2011.
[42] A.E. Morishige, H.S. Laine, J. Schön, A. Haarahiltunen, J. Hofstetter, C. del Canizo, M.C. Schubert, H. Savin, T. Buonassisi, Building intuition of iron evolution during solar cell processing through analysis of different process models, Appl. Phys. A: Mater. Sci. Process. 120 (2015) 1357–1373.
[43] M. Kittler, W. Seifert, Estimation of the upper limit of the minority-carrier diffusion length in multicrystalline silicon: limitation of the action of gettering and passivation on dislocations, Solid State Phenom. 95–96 (2004) 197–204.
[44] J. Isenberg, J. Dicker, W. Warta, Averaging of laterally inhomogeneous lifetimes for one-dimensional modeling of solar cells, J. Appl. Phys. 94 (2003) 4122–4130.
[45] B. Michl, M. Rüdiger, J.A. Giesecke, M. Hermle, W. Warta, M.C. Schubert, Efficiency limiting bulk recombination in multicrystalline silicon solar cells, Sol. Energy Mater. Sol. Cells 98 (2012) 441–447.
[46] H. Wagner, M. Müller, G. Fischer, P.P. Altermatt, A simple criterion for predicting multicrystalline Si solar cell performance from lifetime images of wafers prior to cell production, J. Appl. Phys. 114 (2013) 054501.
[47] S.M. Scott, J. Hofstetter, A.E. Morishige, T. Buonassisi, A sacrificial high-temperature phosphorus diffusion gettering process for lifetime improvement of multicrystalline silicon wafers, Conference Rec. of the 40th IEEE Photovolt. Specialists, Denver, USA, pp. 3014–3016, 2014.
[48] M. Al-Amin, J.D. Murphy, Increasing minority carrier lifetime in as-grown multicrystalline silicon by low temperature internal gettering, J. Appl. Phys. 119 (2016) 235704.
[49] H. Wagner, A. Dastgheib-Shirazi, B. Min, A.E. Morishige, M. Steyer, G. Hahn, C. del Cañizo, T. Buonassisi, P.P. Altermatt, Optimizing phosphorus diffusion for photovoltaic applications: peak doping, inactive phosphorus, gettering, and contact formation, J. Appl. Phys. 119 (2016) 185704.
[50] A. Youssef, J. Schön, T. Niewelt, S. Mack, S. Park, K. Nakajima, K. Morishita, R. Murai, M.A. Jensen, T. Buonassisi, M.C. Schubert, Swirl defect investigation using temperature- and injection-dependent photoluminescence imaging, Conference Rec. of the 43rd IEEE Photovolt. Specialists, Portland, USA, pp. 1303–1307, 2016.
[51] B. Sopori, S. Devayajanam, P. Basnyat, T. Tan, A. Upadhyaya, A. Rohatgi, H. Xu, Dissolution of oxygen precipitate nuclei in n-type CZ-Si wafers to improve their material quality: experimental results, J. Photovolt. 7 (2017) 97–103.
[52] V. LaSalvia, M.A. Jensen, A. Youssef, W. Nemeth, M. Page, T. Buonassisi, P. Stradins, Utilization of tabula rasa to stabilize bulk lifetimes in n-Cz silicon for high-performance solar cell processing, Conference Rec. of the 43rd IEEE Photovolt. Specialists, Portland, USA, pp. 1047–1050, 2016.
[53] K. Hartman, M. Bertoni, J. Serdy, T. Buonassisi, Dislocation density reduction in multicrystalline silicon solar cell material by high temperature annealing, Appl. Phys. Lett. 93 (2008) 122108.